

AN UNUSUAL OUTFLOW AROUND IRAS 16293-2422

CHRISTOPHER K. WALKER, CHARLES J. LADA, ERICK T. YOUNG, AND MICHAEL MARGULIS

Steward Observatory, University of Arizona

Received 1987 August 20; accepted 1988 February 29

ABSTRACT

We have observed the dense, dusty molecular cloud core associated with the unusual protostellar source IRAS 16293-2422 (IRAS 1629A) in the $J = 2 \rightarrow 1$ transition of ^{12}CO and ^{13}CO . These observations indicate that IRAS 1629A is a source of an unusual high-velocity molecular outflow. The outflow possesses four separate emission lobes. The morphology and velocity structure of the lobes may suggest the presence of a dual jet or double bipolar outflow system originating from the vicinity of IRAS 1629A. Our observations resolve the outflowing gas into numerous high-velocity clumps which are either being continuously accelerated from low to high velocity along the entire length of the flow or are undergoing free-flow expansion.

Subject headings: infrared: sources — nebulae: individual (ρ Oph) — nebulae: internal motions — stars: pre-main-sequence.

I. INTRODUCTION

It has become increasingly apparent over the past few years that a large number of young stars undergo a period of mass loss characterized by cold, energetic outflows of molecular gas (Lada 1985). One of the most active regions of star formation known is the Rho Ophiuchi cloud complex. If the outflow phenomena is truly an integral part of the star formation process, it is likely that this region should contain a large number of them. However, until 1985, no definitive detections of molecular outflows have been reported in Rho Ophiuchi. This motivated us to perform a systematic search for molecular outflow activity around known infrared and far-infrared sources in the Rho Ophiuchi region. Observations of the ^{12}CO $J = 2 \rightarrow 1$ transition were made toward a large number of sources, two of which appeared to have high-velocity CO line wings. The most prominent outflow was associated with an isolated and unusual IRAS source located in the eastern streamer region of the Rho Ophiuchi cloud complex (Walker *et al.* 1985; see also Wotton and Loren 1987; Fukui *et al.* 1987). Subsequent observations of this source at millimeter wavelengths have shown it to possess some unusual properties.

Very strong CS emission is found to peak on the IRAS source indicating the presence of dense molecular gas toward the source (Walker *et al.* 1986). Deep self-reversals and prominent asymmetries were found to characterize the C^{32}S emission line profiles, suggesting the presence of systematic velocity fields around the IRAS source. Initial analysis of C^{32}S and C^{34}S spectra suggested infall motions as the origin of the structure in the observed profiles (Walker *et al.* 1986). Subsequent observations and analysis appear to suggest a more complex interpretation, which could also include the possibility that rotation (Menten *et al.* 1987) or perhaps even outflow motions (Walker *et al.* 1988) are significantly affecting the observed line shapes.

A C^{32}S $J = 5 \rightarrow 4$ map of the region indicates that the dense gas is contained in an elongated, molecular core more or less centered on the source. In addition continuum data taken at 1.3 mm and 2.7 mm indicate the presence of cold, dense, dust surrounding the IR object (Walker *et al.* 1986; and Mundy, Wilking, and Myers 1986). Partially resolved observations of the dust at 2.7 mm show an elongated, disklike structure which

is oriented in roughly the same direction as the elongated molecular core.

In this paper we will present our observations of the unusual outflow emanating from the IR source and discuss its properties.

II. OBSERVATIONS

IRAS 1629A ($\alpha = 16^{\text{h}}29^{\text{m}}20^{\text{s}}.9$, $\delta = -24^{\circ}22'13''$) was observed in the $J = 2 \rightarrow 1$ rotational transition of ^{12}CO and ^{13}CO . The observations were made in 1985 March, June, and December with a cooled dual channel, mixer receiver at the NRAO¹ 12 m millimeter wave telescope. Two 512 channel filter bank spectrometers were used, one with 250 kHz channel bandwidths and the other with 500 kHz channel bandwidths. The filter banks were split so that each polarization channel of the receiver coupled to two independent 128 channel banks of 250 kHz and 500 kHz filters. All spectra were observed in the beam-switching mode using an off position which was found to be free of significant molecular line emission at the frequency of interest. Initial calibration of all data was achieved using the chopper wheel calibration technique described by Ulich and Haas (1976). The spectra and maps are presented in terms of T_{R}^* . In addition sky tips were made frequently during the observations to determine the atmospheric optical depth, τ , which was later used to compensate for the elevation dependence of the calibration factor T_{C} .

III. RESULTS

a) Morphology

The $^{12}\text{C}^{16}\text{O}$ $J = 2 \rightarrow 1$ transition was observed at 132 positions around IRAS 1629A. The observed positions were $20''$ apart (the beam size was $27''$) and formed a grid $280''$ by $200''$ approximately centered on the IR source. The spectra, in general, have a single peak at a velocity of 4.0 km s^{-1} and broad emission wings. The velocity extent of the emission wings is about 40 km s^{-1} suggesting that an energetic outflow is responsible for the high-velocity gas (e.g., Lada and Harvey 1981).

¹ The National Radio Astronomy Observatory is operated by Associated Universities Inc., under contract to the National Science Foundation.

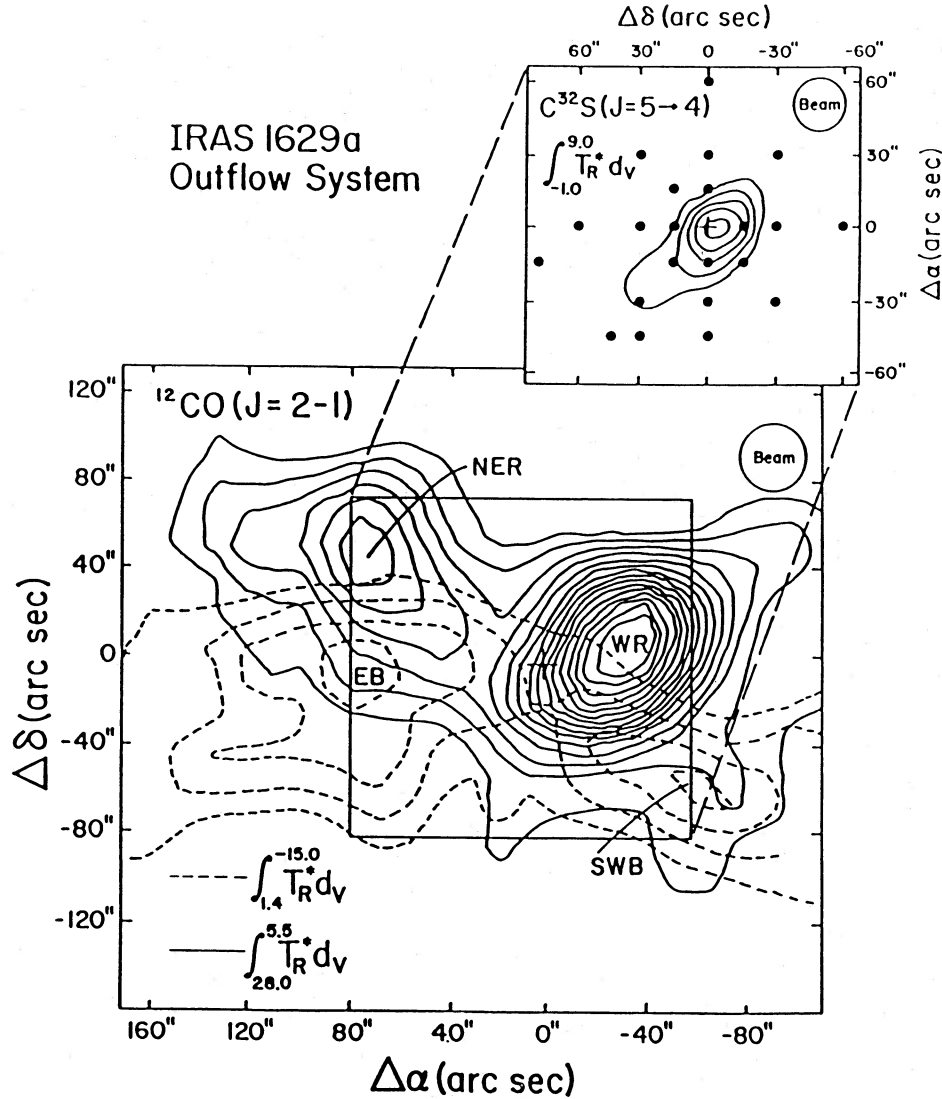


FIG. 1.—Contour map of the integrated intensity of the outflow system around IRAS 1629A. The contour interval is 5 K km s^{-1} . The contours extend from 6 to 26 K km s^{-1} for the blueshifted gas and 11 to 36 K km s^{-1} for the redshifted gas. A cross indicates the position of the far-IR source. The four outflow lobes are labeled according to their position and Doppler shift: *EB* (Eastern Blue), *WR* (Western Red), *SWB* (Southwestern Blue), and *NER* (Northeastern Red). The rms noise level is $\sim 1.0 \text{ K km s}^{-1}$. The CS ($J = 5 \rightarrow 4$) core observed toward the far-IR source is shown in projection and is from Walker *et al.* (1986). The contour limits are 3.5 K km s^{-1} and 7.5 km s^{-1} . The contour interval is 1 K km s^{-1} . Filled circles indicate observed positions and the “+” indicates the position of the far-IR source.

In order to investigate the spatial distribution of the high-velocity gas about the source, a contour map (Fig. 1) was made of the integrated “red” and “blue” wing emission at each position in the grid. Here we define the red and blue emission as follows:

$$\text{RED} = \int_{5.5 \text{ km}^{-1}}^{28.0 \text{ km}^{-1}} T_v^{12} dv \quad \text{BLUE} = \int_{-18.0 \text{ km}^{-1}}^{1.4 \text{ km}^{-1}} T_v^{12} dv. \quad (1)$$

In general, if the blue and red emission peaks are spatially separated, then the presence of a bipolar outflow is indicated. Inspection of Figure 1 indicates that not only are the emission peaks spatially separated, but that there are two separate red emission lobes and two separate blue emission lobes. The eastern blue (*EB*) lobe and western red (*WR*) lobe appear to be rounder in shape than the northeastern red (*NER*) lobe and southwestern blue (*SWB*) lobe. Let us define a collimation

factor CF such that $CF = L/W$, where L equals the maximum half-power length of the lobe, and W equals the maximum half-power width of the lobe. Then we find that *EB*, *WR*, *SWB*, and *NER* have collimation factors of 2.0, 1.4, 2.5, and 2.5, respectively. Lobes *NER* and *SWB* appear to be better collimated than lobes *EB* and *WR*. The inset shows the CS $J = 5 \rightarrow 4$ map from Walker *et al.* (1986) for comparison.

An outflow system possessing a very similar morphology was observed in the $^{12}\text{CO } J = 1 \rightarrow 0$ line by Goldsmith *et al.* (1984) and Hayashi *et al.* (1987) toward the infrared source L723. However, this outflow’s kinematics have not yet been studied in detail.

b) The Structure of the Outflow Velocity Field

In order to investigate the detailed variation in the outflow spatial-velocity field, contour maps were constructed of integrated intensities obtained for small velocity intervals across the line profiles. The emission across each profile was inte-

grated over contiguous velocity intervals, each 3.25 km s^{-1} (or five, 0.65 km s^{-1} filterbank channels) in extent. The resulting 3.25 km s^{-1} resolution maps are displayed in Figure 2. From left to right, the individual maps are referred to as Figures 2a–2l. The contour map parameters are given in Table 1. The systematic velocity of the cloud is 4.0 km s^{-1} , the velocity at which the peak in the CO emission profile is usually found.

Figure 2g shows the map of emission integrated over the cores of the observed line profiles. The emission presumably arises from ambient gas, yet it does not peak up on the infrared source, which is located in the densest part of the cloud and is clearly the dominant energy source in the region (Walker *et al.*

1986). Instead the emission peaks near the positions of the strongest red and blueshifted lobes in the outflow (see Fig. 1). Indeed, this is found to be true even in maps made from the individual velocity channels (0.65 km s^{-1} resolution) throughout the line core. This result does not appear to be affected by the very narrow ($\leq 0.65 \text{ km s}^{-1}$) and relatively shallow self-absorption which is present in some profiles. Therefore, it appears that the outflow significantly contributes to the observed emission even at the ambient gas velocities in the line core.

We have made measurements of the half-intensity sizes of the mapped region as a function of velocity, using the various

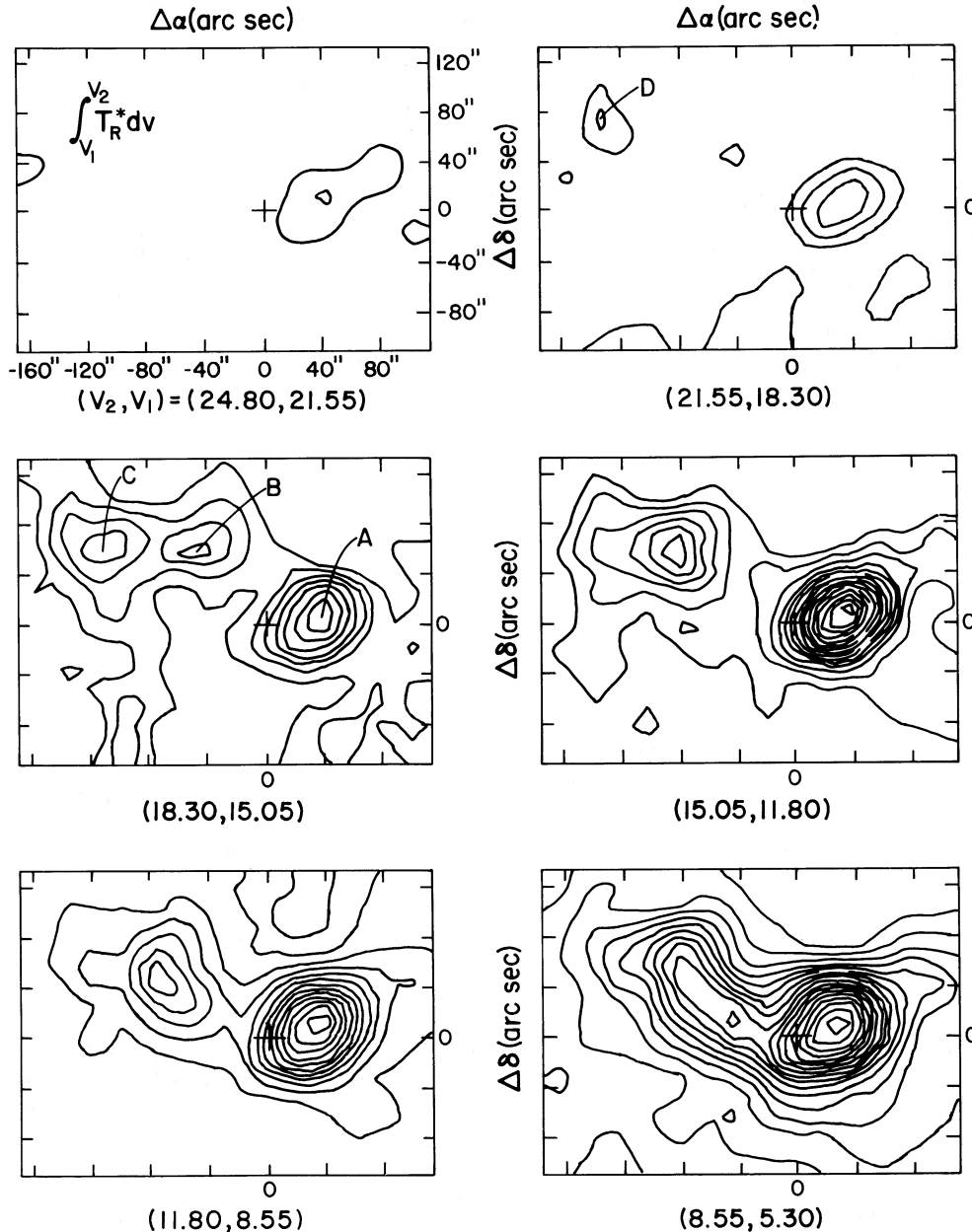


FIG. 2.—Integrated intensity of the outflowing gas as a function of velocity. Each observed line profile was integrated over contiguous velocity intervals, each 3.25 km s^{-1} (or five, 0.65 km s^{-1} filterbank channels) in extent. The limits of integration are indicated for each map in V_{LSR} . The rest velocity of the cloud is 4 km s^{-1} . Due to the large dynamic range of the integrated intensity in the various velocity bins, the contour limits and intervals are different for each map and are given in Table 2. The distance between tick marks is $20''$, which corresponds to the spacing between observed positions. The position of the far-IR source is indicated by a cross and is the (0, 0) point of our maps. The locations of the high-velocity clumps A–J are also indicated. From left to right the individual maps are referred to as Figs. 2a–2l.

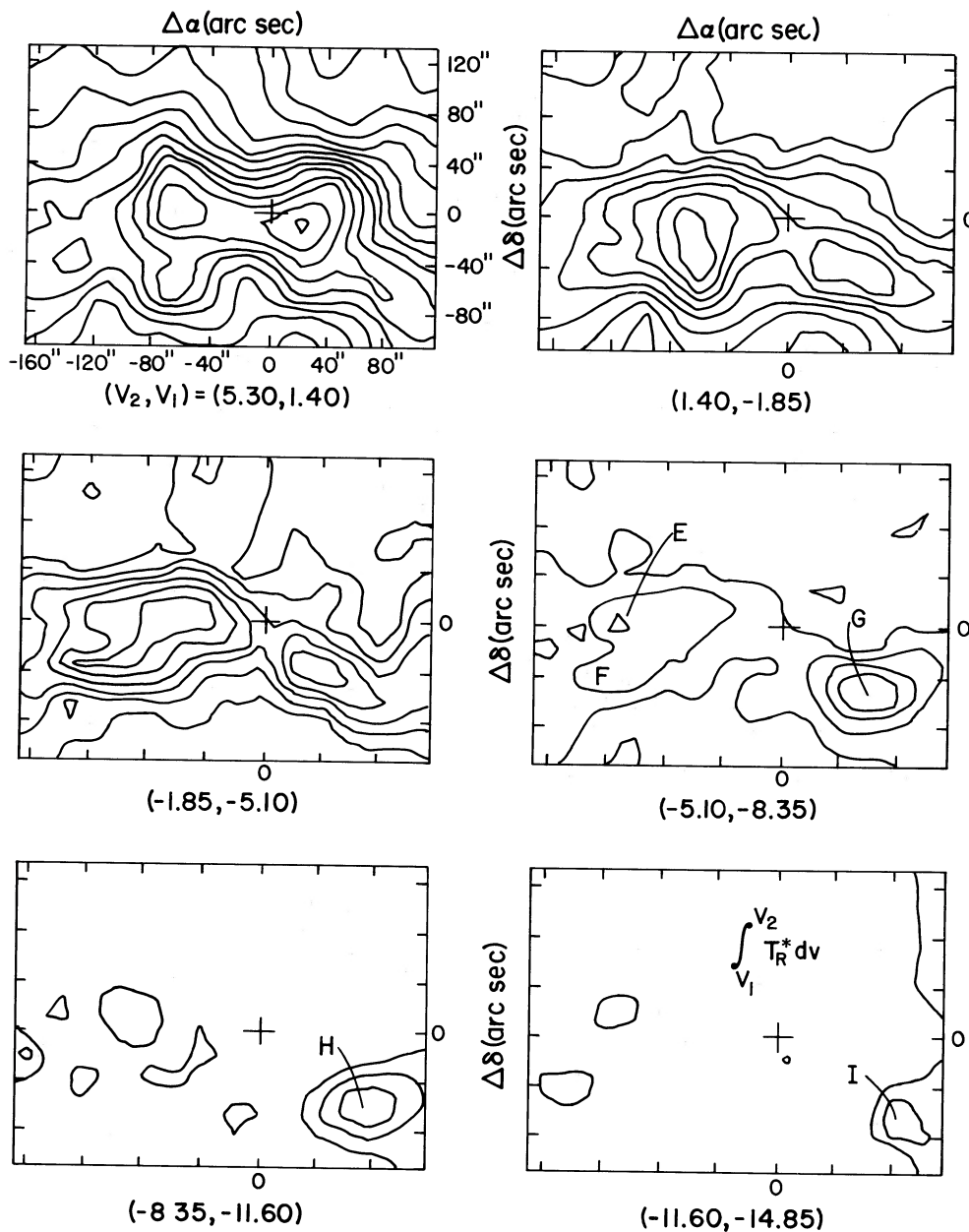


FIG. 2—Continued

maps in Figure 2, and in the core region, using contour maps made for the individual 0.65 km s^{-1} velocity channels. We find that at velocities between 2 and 5 km s^{-1} a significant contribution to the line emission arises from an extended emission region. But, at velocities greater than 5 km s^{-1} and less than 2 km s^{-1} , the half-power source size falls abruptly. For velocities greater than 5 km s^{-1} the emitting gas is always found to encompass an area between 1000 and 3000 square arc seconds with the smaller flow sizes occurring at the higher velocities. Thus, the outflow becomes clearly distinct from the ambient gas at velocities greater than 5.0 km s^{-1} and less than 2 km s^{-1} . Even though the presence of the outflow noticeably affects the line intensities even in the cores of the observed line profiles, the bulk of the observed emission, between 2 and 5 km s^{-1} , still arises from ambient gas.

Examination of Figures 2f and 2h shows that at the lowest

discernable outflow velocities relative to line center, CO emission can be detected and is more or less smoothly distributed throughout the observed extent of the flow. However, at higher flow velocities (Figs. 2a-e and 2i-l) the emission breaks up into what appear to be narrower distinct clumps. As many as nine high-velocity clumps (labeled A-I in Fig. 2) can be identified in the red and blue lobes at velocities greater than 10 km s^{-1} from line center.

Careful inspection of the maps in Figure 2 shows an intriguing tendency for emission at increasing positive (redshifted) and increasing negative (blueshifted) velocities in lobes *NER*, *SWB*, and *EB* to be located at systematically increasing distances from the embedded infrared source (IRAS 1629A). Particularly striking are lobes *NER* and *SWB*, which with increasing velocity become more and more detached from the east-west lobes and each other until at the highest velocities,

TABLE 1
CONTOUR MAP PARAMETERS FOR FIGURE 2

MAP	CONTOURS (K km s ⁻¹)		
	min	max	interval
a.....	1	2	1
b.....	1	3	1
c.....	1	7	1
d.....	1	15	1
e.....	0	22	2
f.....	1	33	2
g.....	16	40	2
h.....	1	15	2
i.....	1	6	1
j.....	1	4	1
k.....	1	3	1
l.....	1	2	1

independent clumps of emission (*D* and *G*) located at the edges of an apparent northeast-southwest axis clearly appear. Although less dramatic, a similar trend is observed for lobe *EB*. The variation of the position of peak emission as a function of velocity for each of the four lobes is also shown in Figure 3. Here we plot the postional centroids of all significant emission peaks in each of the maps in Figure 2. This particular representation of the data clearly shows that as the velocity increases, the spatial peaks of the emission move progressively away from the IR source for lobes *NER*, *SWB*, and *EB*. Comparison

of Figures 2 and 3 show that the clumpy nature of the outflow emission is apparent even at the lower outflow velocities. Evidence for gas motions similar to that discussed above has also been observed toward L1551 by Fridlund *et al.* (1984) and Moriarty-Schieven *et al.* (1986).

c) Outflow Mass and Energetics

Both ¹²CO *J* = 2 → 1 and ¹³CO *J* = 2 → 1 observations were made toward the infrared source. The spectra are shown in Figure 4. Extended wing emission can be seen on both the red and blueshifted sides of the ¹²CO line. As indicated in Figure 5, the emission drops off more sharply at low velocities on the blueshifted side of the line than on the redshifted side. This suggests that on the redshifted side of the line, emission from the outflow extends in velocity space almost all the way up to line center. In the ¹³CO line profile, only the redshifted low-velocity wing emission was strong enough to be detected above the relatively high rms noise level (0.135 K) of the data. This appearance is probably due to the fact that although the infrared source is located (at least in projection) inside the boundary of lobe *WR*, it is in a position directly in between the peaks of the two blue lobes, where there is a relatively low amount of blueshifted emission (see Fig. 1 and 2).

If we assume that the ¹²CO wing emission is optically thick, then the mass of the material in the wings can be estimated from the ¹²CO and ¹³CO data over the velocity interval that ¹³CO wing emission is observed ($V_{\text{LSR}} = 5.3\text{--}11.0$ km s⁻¹). No effort will be made to estimate the mass of the outflow material

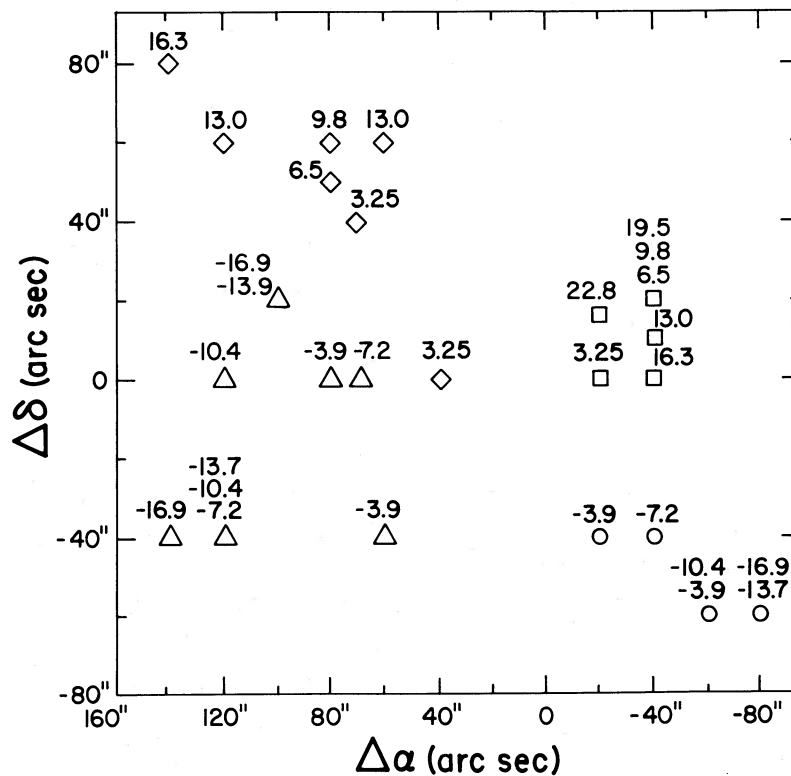


FIG. 3.—Spatial distribution of emission peaks as a function of velocity. The position of the emission peaks in the outflow lobes are indicated by a diamond for lobe *NER*, a "○" for lobe *SWB*, a square for lobe *WR*, and a triangle for lobe *EB*. The velocity of the emission peaks relative to line center are given above each symbol. Since the 3.25 km s⁻¹ resolution maps of Figure 2 were used to produce this diagram, these velocities indicate the mean velocity of the gas in each emission peak. When the position of an emission peak was the same for more than one velocity, these velocities are shown. The far-IR source is located at position (0, 0).

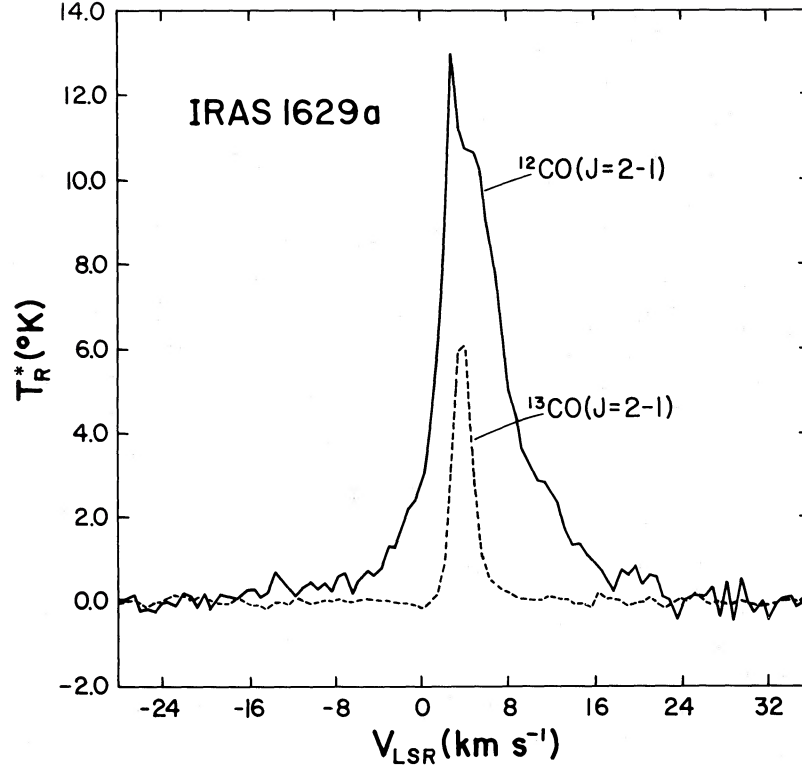


FIG. 4.— ^{12}CO and ^{13}CO $J = 2 \rightarrow 1$ spectra taken toward the far-IR source IRAS 1629A

“hidden” in the line core. The mean optical depths for both isotopic emission lines can be found from the ratio of the ^{12}CO and ^{13}CO line intensities if it is assumed that $\tau_{12} = 89\tau_{13}$ and both transitions have identical excitation temperatures (Bally and Lada 1983). The value of τ_{13} can then be used to calculate the excitation temperature T_{ex} of the ^{13}CO gas:

$$\frac{T_R^{13}}{f} = [J_\nu(T_{\text{ex}}) - J_\nu(T_{\text{bg}})] [1 - \exp(-\tau_\nu^{13})], \quad (2)$$

where

$$J_\nu(T) = \frac{h\nu}{k} \left[\exp\left(\frac{h\nu}{kT}\right) - 1 \right]^{-1}$$

$$T_R^{13} = \frac{(T_R^*)^{13}}{\eta_c}$$

T_R^{13} is the source radiation temperature (Kutner and Ulich 1981). The value η_c is the coupling efficiency between the telescope and the outflow, which we take to be ~ 0.5 (Ulich and Haas 1976).

In order to determine an accurate value for T_{ex} , an estimate of the gas filling factor f is needed. To determine an accurate value for f , CO observations are required in at least two different transitions. Unfortunately, we have data only for the $J = 2 \rightarrow 1$ transition. However, Snell *et al.* (1984) and Margulis and Lada (1985) have found that, in general, the filling factor in outflows approaches 1 at velocities near that of the line core. Since we are calculating the mass of relatively low-velocity material in the outflow system, we will adopt this value.

Once obtained, the value of T_{ex} can be used to determine the

^{13}CO column density at each velocity in the line profile. For the $J = 2 \rightarrow 1$ transition the required expression is

$$N_V^{13} = 1.25 \times 10^{14} \tau_\nu^{13} (T_{\text{ex}} + 0.91) \exp\left(\frac{h\nu}{2kT_{\text{ex}}}\right) \left[1 - \exp\left(\frac{-h\nu}{kT_{\text{ex}}}\right) \right]^{-1}. \quad (3)$$

The total ^{13}CO column density is then found by integrating N_V^{13} over the wing velocity interval (ΔV) of interest. The corresponding value for the column density of hydrogen N_{H_2} is determined using the ^{13}CO to H_2 abundance ratio of Dickman (1978), $N_{\text{H}_2} = N^{13}/2.5 \times 10^{-6}$. The total mass of H_2 molecules in the flow can be found by integrating N_{H_2} over the total flow area. Since we have only a single ^{13}CO observation toward the source of the flow, a ^{12}CO emission weighted area A_w is used in the integration. If we assume that the ^{12}CO optical depth and H_2 column density are proportional to the observed ^{12}CO integrated intensity at each position, then the value of A_w should reflect the variation of N_{H_2} over the flow region:

$$A_w = \int_{\text{flow}} \frac{I^{12} d\alpha d\delta}{I_{\text{center}}^{12}}, \quad (4)$$

where the integrated intensity I^{12} is given by

$$I^{12} = \int_{v_1}^{v_2} T_\nu^{12} dv.$$

The flow mass is then given by (Margulis and Lada 1985)

$$\frac{M}{M_\odot} = 1.60 \times 10^{-20} N_{\text{H}_2} (\text{cm}^{-2}) A_w (\text{pc}^2). \quad (5)$$

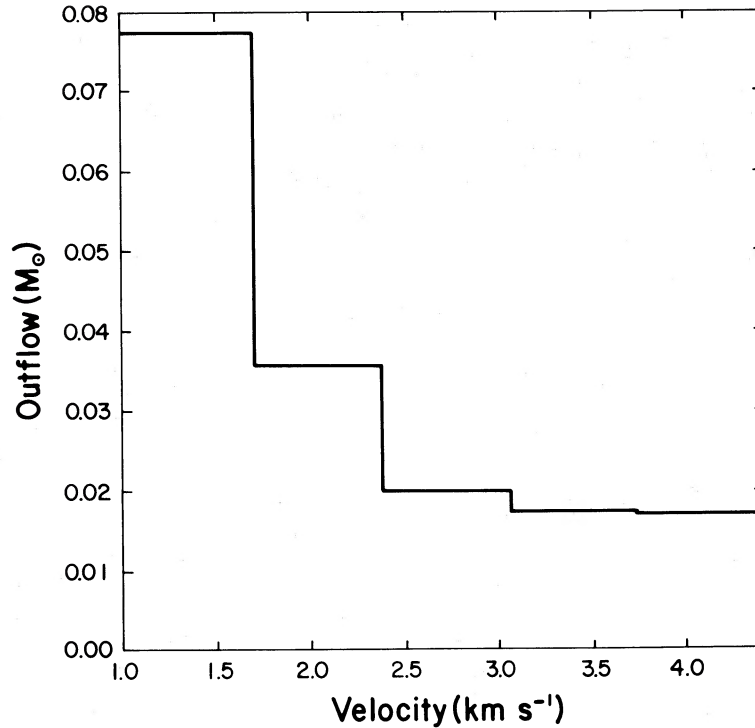


FIG. 5.—Mass of the redshifted outflow gas as a function of velocity. These masses were computed on a channel by channel basis using the ratio of ^{12}CO to ^{13}CO line temperatures as described in the text.

As previously discussed only a red emission wing was observed in the ^{13}CO line profile. Therefore mass estimates derived from the ratio of ^{12}CO and ^{13}CO line temperatures as described above can only be made for the redshifted outflow regions. Masses were calculated using this technique in two ways.

1. The total mass of the redshifted gas was computed by using a value of T_{ex} (15.9 K) that was found by averaging the single filterbank channel values of temperature over the observed red wing, and using a value of ΔV equal to the total observed velocity extent of the wing (6 km s^{-1} relative to line center).

2. A mass was also computed for each filterbank channel in the ^{13}CO red wing out to a velocity of $\sim 3.25 \text{ km s}^{-1}$ from line center. In these mass estimates we adopted a value for T_{ex} (20 K) equal to the arithmetic mean of the individual channel values of T_{ex} calculated over the innermost 2 km s^{-1} of the wing. At these low outflow velocities our assumption of a unity filling factor is more likely to be correct. Mass calculations at larger velocities were prohibited by the noise level of the observations.

The mass obtained by averaging over the red wing (method 1) was $M_{\text{Red}} = 0.27 M_{\odot}$. Averaging out to 6 km s^{-1} from line center may lead to an underestimate of T_{ex} since the filling factor may be less than 1. If, instead, the 20 K excitation temperature found using method 2 is used, then the mass is estimated to be $0.37 M_{\odot}$. A plot showing the estimated mass of the redshifted outflow as a function of velocity is given in Figure 5. If the mass calculated for each channel, m_{ch} , is simply added together such that

$$M_{\text{Red}} = \sum_{\text{ch}=58}^{62} m_{\text{ch}} \quad (6)$$

one finds $M = 0.17 M_{\odot}$, a value $-\frac{1}{2}$ times that calculated by averaging over the wing, assuming $T_{\text{ex}} = 20 \text{ K}$. It is interesting to note that the velocity extent over which masses were calculated using method 2 were twice that used in method 1. This implies that the relationship between velocity and mass may be linear.

These mass estimates are lower limits since the contributions from the low-velocity outflow gas in the line core and at high velocities where ^{13}CO was not observed are not included. However, if we assume that the ^{12}CO to ^{13}CO integrated intensity ratio is constant with velocity and position, and equal to the value observed toward the infrared source over the range of velocities where ^{13}CO was detected, then the total mass of the outflowing gas in the ^{12}CO profile can be estimated by calculating a value of A_w corresponding to the emission from the red and blueshifted gas and utilizing equation (5). When this is done one finds that the total mass of high-velocity red and blueshifted gas is 0.5 and $0.3 M_{\odot}$ respectively. From a comparison of the emission weighted areas for lobes *NER*, *EB*, *WR*, and *SWB*, we find that the mass of material in lobes *EB* and *WR* is on the average a factor of 2 greater than the mass of material found in lobes *NER* and *SWB*. This technique can also be used to determine the mass (M_{cl}) of a gas clump at any velocity or position in the outflow, i.e.,

$$M_{\text{cl}} = 2m_{\text{H}} A_w N_s \quad (7)$$

where N_s is the H_2 column density derived for the red wing from the ^{12}CO and ^{13}CO observations of the central source. A_w is the clump emission weighted area, calculated over the appropriate velocity interval. Mass estimates for clumps *A-I* were made using this technique, and are listed in Table 2 along with the clump radii. These represent lower limits since A_w was

TABLE 2
CLUMP CHARACTERISTICS

Clump (1)	Velocity (km s ⁻¹) (2)	Radius (× 10 ¹⁶ cm) (3)	Mass (× 10 ⁻³ M _⊙) (4)
A	12.7	6.7	23
B	12.7	5.9	5.7
C	12.7	7.3	23
D	15.9	3.8	1.3
E	10.7	8.6	29
F	10.7	6.1	6.0
G	10.7	6.2	14.3
H	14.0	6.4	10.5
I	17.2	5.4	4.6

calculated within each clump's half-power contour. A plot of clump mass as a function of velocity is given in Figure 6. Clump masses were found to range from 0.023 to 0.0002 M_⊙, with the smallest clump masses occurring at high velocities. From summing up the individual clump masses in Table 2, one finds that ~15% of the total mass of the outflow is contained in high-velocity clumps.

Estimates of the momentum contained in an outflow can be found by multiplying the obtained mass by some characteristic outflow velocity V . The amount of kinetic energy in the outflow is found by multiplying the mass estimate by $\frac{1}{2}V^2$. However, since we have knowledge only about the radial component of the outflow velocity, we can only estimate the momentum and energy of the outflow directed along our line of sight.

When calculating the flow's momentum and energy using the total estimated mass M_{total} , V was set equal to the maximum observed velocity V_{max} in the ¹²CO $J = 2 \rightarrow 1$ line profile, ~16 km s⁻¹. By using this value for V one assumes that all material in the flow is moving at the maximum observed velocity and all lower observed flow velocities are produced by projection effects. This technique provides an upper limit to the flow's momentum and energy.

When calculating the flow's momentum and energy individually for each filter bank channel, V is set equal to the velocity of the channel relative to line center (Snell *et al.* 1984). This technique assumes that the actual velocity of the material is the same as the observed radial velocity. By summing the momentum and energy over all the channels, estimates of the total momentum, P , and kinetic energy, KE, in the flow can be made

$$P = \sum_{\text{ch}} m_{\text{ch}} v_{\text{ch}}, \quad \text{KE} = \frac{1}{2} \sum_{\text{ch}} m_{\text{ch}} v_{\text{ch}}^2.$$

Unless the outflow is directed entirely along our line of sight, these estimates will be less than the actual values.

Now if we define a dynamical time scale $\tau_d = R/V$ for the outflow, where R is the linear extent of the outflow as measured from the IR source to the outer half-power contours of the outflow integrated intensity maps, and V is defined as described above, then the average force needed to drive the outflow (the momentum supply rate), $\dot{P} = P/\tau_d$, and the mechanical luminosity of the flow (energy supply rate), $L = \text{KE}/\tau_d$, can be calculated.

Table 3 lists the values of M_{tot} , P , KE, \dot{P} , and L derived using the total estimated mass of the outflow and by averaging over

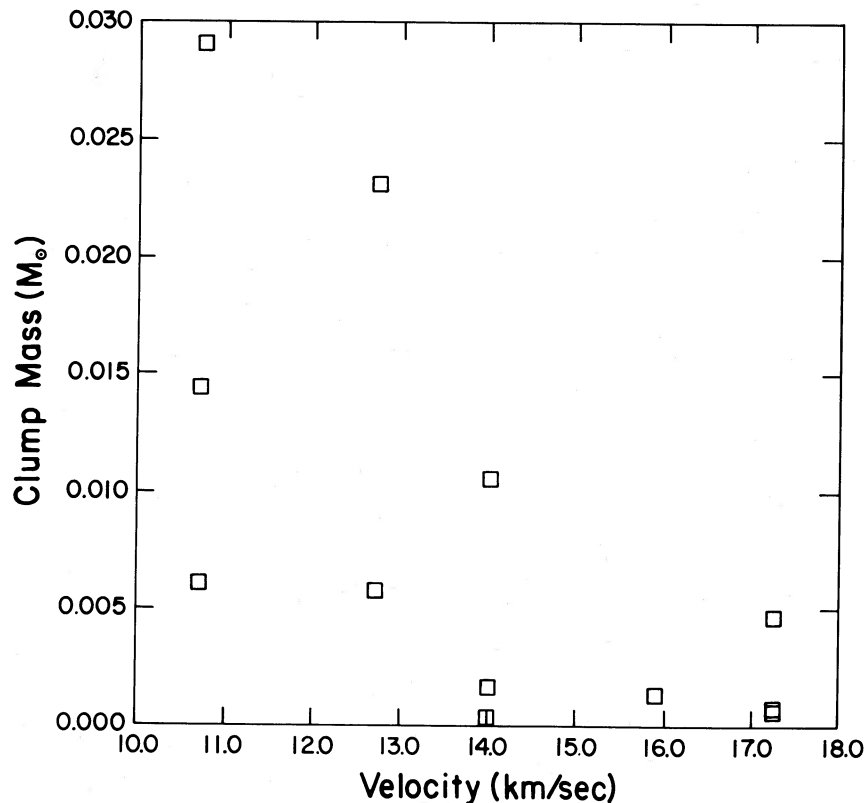


FIG. 6.—High-velocity clump mass as a function of velocity from line center. The clump masses were computed assuming the column density of H₂ toward each clump was the same as that derived for the redshifted gas from the ¹²CO and ¹³CO observations of the central source.

TABLE 3
OUTFLOW CHARACTERISTICS

Parameter	Averaged over Red Wing	Summed over Red Wing Channels	For Entire Outflow System
$M_{\text{tot}} (M_{\odot})$	0.27	0.17	0.8
$P (M_{\odot} \text{ km s}^{-1})$	4.32	0.36	12.8
$\text{KE} (M_{\odot} \text{ km}^2 \text{ s}^{-2})$	34.6	0.46	102.4
$\dot{P}/L_{*}/c$	1153	25.0	3412
L/L_{\odot}	0.71	0.003	2.1
$\dot{P} (M_{\odot} \text{ yr}^{-1} \text{ km s}^{-1})$	5.5×10^{-4}	1.17×10^{-5}	1.63×10^{-3}

the red wing and summing individual channel values for the combination of the two redshifted lobes (*WR* and *NER*) observed toward IRAS 1629A. The value of τ_d found by setting $V = V_{\text{max}}$ was 8000 yr. The value of τ_d found by setting $V = v_{\text{ch}}$ ranged from 17,000 to 58,000 yr. Jets *WR* and *NER* are found to have a combined mechanical luminosity of only a small fraction of $1 L_{\odot}$, while the infrared source driving the flow has a bolometric luminosity of $L = 23 L_{\odot}$. The ratio of \dot{P} to L/c (the ratio of the momentum flux needed to drive the outflow to the momentum flux of the photons from the IR source) is found to range from 25 to 1153 depending on whether it is computed separately for individual channels or by using the total mass of the red wing ($0.27 M_{\odot}$) and V_{max} . The large value of this ratio appears to indicate that the radiation pressure from the IR source cannot drive the outflow (Bally and Lada 1983).

IV. DISCUSSION

a) The Nature of the Outflow System

As discussed earlier, IRAS 1629A has twice the number of red and blueshifted emission lobes as a "classical" outflow system (e.g., L1551). There are at least four possible interpretations of this observation. (1) There are two separate bipolar outflows present. The *NER* and *EB* lobes forming one pair and the *WR* and *SWB* lobes forming another. IRAS 1629A is not driving either flow. (2) There is a single bipolar outflow with a large opening angle driven by IRAS 1629A. This outflow consists of two limb brightened, cone-shaped, rapidly rotating lobes (*NER* and *EB*, and *WR* and *SWB*, respectively) each of which contains both red and blueshifted gas due to the rotation. (3) There is a single bipolar outflow with a large opening angle as in (2), but the lobes are not rotating and lie mostly in the plane of the sky. Here the presence of the red and blueshifted emission in the same outflow lobe is due to the combination of a large opening angle and our line of sight relative to the outflow axis. (4) There are two separate bipolar flows, each being driven by IRAS 1629A, *NER* and *SWB* making one pair and *EB* and *WR* the other.

The nearly constant acceleration of molecular gas away from IRAS 1629A observed in three of the four lobes (Fig. 3) coupled with the lack of any other infrared sources in the field, strongly implicates IRAS 1629A as the driving source of the high-velocity molecular flow and makes (1) untenable.

Rotating outflow lobes (alternative [2]) are predicted by certain theoretical models in which the outflows are driven outward along wound-up magnetic field lines threading rotating magnetized disks (Uchida and Shubata 1985; Pudritz and Norman 1983). However, the observed velocity difference between the outflow lobes cannot possibly be attributed to rotation, since the implied rotation rate is greatly in excess of

that which can be confined by ambient cloud gravity, or magnetic, turbulent, or thermal pressure. For example, a magnetic field of $\sim 10^{-3}$ gauss or a gravitational mass of $3000 M_{\odot}$ would be required.

If the outflow's opening angle is large and its inclination to the plane of the sky is small, it may be possible that a combination of limb brightening and line-of-sight effects could be responsible for the unusual geometry of the outflow system (alternative [3]). Cabrit and Bertout (1986) show how the line of sight through a filled outflow lobe can cause both blue and redshifted emission to be observed toward the same position (case 3 and 4 of their models). Since the outflow lobes were assumed to be filled, the emission in their models tends to peak along the outflow axis. However, in the case of IRAS 1629A, the emission is found to peak along the edges of the flow, suggesting the presence of a shell source around an outflow cavity, which is inconsistent with the predicted morphology of a case 3 or 4 source. Whether modifying the model to account for shell structures could produce the observed spatial displacement in red and blueshifted emission in the same outflow lobe without the presence of rotation is, at present, unclear.

Another possible explanation of the observations is that there are two separate bipolar outflows or jets emanating from the vicinity of IRAS 1629A. The morphology and velocity structure suggest that the two narrow lobes and round lobes respectively define outflow axes which intersect within $10''$ of the position of IRAS 1629A. The axis which connects the two narrow lobes *NER* and *SWB* has a position angle of 51° (measured counterclockwise from north). The other flow axis runs roughly east-west at a position angle of 95° and connects the two "round" lobes *EB* and *WR*. However, this interpretation is not without its own difficulties. How can a single object drive two separate outflows? It is possible that IRAS 1629A may itself be a double source. The extremely high extinction in the vicinity of IRAS 1629A has prevented it from being studied in the near-infrared, and it was undetected by *IRAS* in the $12 \mu\text{m}$ band (Walker *et al.* 1986). High-resolution interferometric observations of the dust continuum at 2.7 mm wavelength have partially resolved the source and show no clear indication of double structure (Mundy, Wilking, and Myers 1986). However, if IRAS 1629A is a binary system, this sets an upper limit of $10''$ or 160 AU to the separation of its members. For a $2 M_{\odot}$ system, the orbital period of the binary would be about 45,000 yr, a period of time between the upper and lower limits of the dynamical age of the outflow. Therefore, if there was a separate bipolar outflow associated with each component of the binary, then the two outflow systems may have already interacted at least once. What the results of such an interaction might be is unknown, but if such an interaction has occurred it would seem unlikely that the resulting outflows would possess as systematic a morphology as that which is observed.

Vrba, Strom, and Strom (1976) have performed extensive polarimetry towards stars in this region of Ophiuchus. The average position angle of the field vectors of all stars within $\sim 20'$ of IRAS 1629A which appear in their study is $57^\circ \pm 7^\circ$, a value very close to that measured for the northeast-southwest outflow axis (51°). If the latter interpretation is correct, this indicates that the northeast-southwest outflow may be aligned with the magnetic field of the cloud. The east-west outflow axis is at an angle of $\sim 37^\circ$ to the magnetic field vector. The apparent alignment of the "narrow" lobes *NER* and *SWB* with the local magnetic field suggests that the field could play an active part in collimating at least part, but not all, of the outflow.

b) Flow Structure and Dynamics

Two of the most interesting aspects of the outflow source are the observation of the increasing displacement of the molecular gas from the infrared source with increasing velocity and the clumpy appearance of the gas at the highest outflow velocities. There are at least two processes which could account for this phenomenon. One is that outflow material is being continuously accelerated from low to high velocities away from the infrared source and that the infrared source may be the driving source of the observed high-velocity motions. The other is that we may be witnessing the free-flow expansion of material after an explosive event. Indeed, if a least-squares fit is made on a plot of clump velocity versus distance, one finds that a y -intercept with a value close to zero is found. If the velocity of each clump has remained constant, this suggests that all the clumps originated at a position close to the infrared source at nearly the same time. However, the systematic displacement of emission peaks with increasing velocity is not obviously present in lobe *WR*, where the locations of peak emission at all velocities are confined to a relatively small region on the map. This may indicate that the outflow axis of lobe *WR* may lie more nearly along our line of sight, or that this jet is relatively young and clumps have not had time to "break out" either as the result of constant acceleration or from free-flow expansion. Evidently the highest velocity material in the flow consists of clumps which have either been accelerated to high velocities along the lobes by a steadily applied force or ejected in a single explosive outburst from the *IRAS* source.

From the CO spectra in Figure 4 and the maps in Figure 2 we estimate that the total mass of all the high velocity ($v \geq 10$ km s $^{-1}$) clumps we have identified is only 15% of the total mass in the outflow. The bulk of the outflowing gas appears smoothly distributed along the various jets at lower velocities. There is also evidence in our data that the sizes of the outflow lobes increases with decreasing velocity. This latter fact suggests that the highest velocity outflow material is located interior to the lower velocity gas.

The fact that the displacement of the highest velocity clumps from the infrared source increases more or less continuously with velocity along the lobes suggests that they are likely located within a relatively low density or possibly evacuated channel or cavity. If the clumps were moving in a channel filled with ambient gas, they would sweep up their own mass by the time they reached the end of the channel if the ambient gas density was equal to

$$n_{\text{amb}} = \frac{M_{\text{cl}}}{2\pi r_{\text{cl}}^2 R_{\text{jet}} m_{\text{H}}} \quad (8)$$

or 3×10^3 cm $^{-3}$ for $M_{\text{cl}} = 0.01 M_{\odot}$, $r_{\text{cl}} = 4 \times 10^{16}$ cm, and

$R_{\text{jet}} = 4 \times 10^{17}$ cm. Since the ambient molecular gas has densities of this order and greater (Walker *et al.* 1988), we would expect to observe low-velocity clumps at the ends of the lobes rather than high-velocity ones.

These considerations suggest a model for the outflow in which the molecular gas is contained in a shell around a low-density or evacuated cavity. As discussed by many authors (e.g., Bally and Lada 1983; Snell *et al.* 1984; Lada 1985) the bulk of the molecular gas observed in a high-velocity outflow is most likely swept-up and accelerated ambient gas rather than the original ejecta from the central source driving the outflow. It has been suggested that an underlying, hot stellar wind (e.g., Snell, Loren, and Plambeck 1980) or a cold disk wind (Uchida and Shibata 1985; Pudritz and Norman 1983) could be the agent which sweeps up the ambient gas and produces the observed molecular outflow. Such winds would be expected to produce wind cavities interior to a swept-up molecular shell. Our observations may provide some new constraints on the physical parameters of these winds.

First, if the high-velocity clumps are being accelerated by a stellar wind, then our data strongly suggest that the wind driving the cold molecular flow must have been a relatively steady wind over the dynamical time of the flow. The nine observed clumps do not appear to be the result of individual intense bursts in an otherwise relatively quiescent wind. In order to accelerate the observed clumps to their high observed velocities (10 km s $^{-1}$) the underlying wind must exert a minimum force, $F \approx (M_{\text{cl}} V_{\text{cl}}^2 / R_{\text{f}})$ where M_{cl} is the clump mass, V_{cl} its observed velocity, and R_{f} the apparent distance over which the clump has been accelerated. For $M_{\text{cl}} = 0.01 M_{\odot}$, $V_{\text{cl}} = 10$ km s $^{-1}$ and $R_{\text{f}} = 4 \times 10^{17}$ cm, $F = 1.0 \times 10^{26}$ dynes. Ram pressure from a stellar wind could produce this force if the wind mass loss rate $\dot{M}_{\text{w}} > 1.6 \times 10^{-7} [V_{\text{w}}/100 \text{ km s}^{-1}]^{-1} M_{\odot} \text{ yr}^{-1}$, and the entire stellar wind were directed into the solid angle of the clump with negligible geometric dilution. For IRAS 1629A, with four jetlike lobes each of which has cross sectional areas that are easily 4 times that of an individual clump a more realistic value for the minimum mass loss rate is $\dot{M}_{\text{w}} > 3 \times 10^{-6} [V_{\text{w}}/100 \text{ km s}^{-1}]^{-1} M_{\odot} \text{ yr}^{-1}$. To drive the entire mass of high-velocity molecular gas the average stellar mass-loss rate would be

$$\begin{aligned} \dot{M}_{\text{w}} &> \frac{\dot{M}_{\text{CO}} V_{\text{CO}}}{V_{\text{w}}} = \frac{\dot{P}}{V_{\text{w}}} \\ &= 1.6 \times 10^{-5} \left[\frac{V_{\text{w}}}{100 \text{ km s}^{-1}} \right]^{-1} M_{\odot} \text{ yr}^{-1}, \quad (9) \end{aligned}$$

where, from Table 3, $\dot{P} \approx 1.6 \times 10^{-3} M_{\odot} \text{ yr}^{-1} \text{ km s}^{-1}$. These considerations suggest that if the observed motions in the high-velocity gas could be produced by a stellar wind which has been steady over the dynamical lifetime of the outflow, then the required mass-loss rate is higher than those inferred for solar mass *T* Tauri stars. This in turn may suggest that the mass-loss rates are much higher and the stellar wind stronger in the protostellar or pre-*T* Tauri phase of early stellar evolution (e.g., Lada 1985). Although it is possible that a modest stellar wind is capable of accelerating the observed clumps, it is not at all clear how such an acceleration could take place, or how such clumps would remain stable and retain their integrity when exposed to such a wind.

Second, as discussed earlier, the clumps may not be accelerating at all, but are instead undergoing a free-flow expansion.

Since the outflow gas at lower velocities is found over the entire extent of the lobes, this low-velocity gas could not have been generated in the same explosive event. In this scenario the low-velocity outflow gas would have to be produced as a result of an accumulation of past explosive events or a steady wind. The high-velocity clumps we are now observing would have been generated from the last outburst. These outbursts could be similar to those seen toward FU Orionis stars. Indeed, Herbig (1977) has estimated that FU Orionis objects may undergo outbursts on time scales of 10^4 yr, a period very close to the dynamical time scale of many outflows (Levreault 1983). Recently several authors have proposed models in which FU Orionis outbursts are repetitive and driven by the accretion of matter onto a protostar (Hartmann and Keyon 1985, 1986; Hanami 1987). For an accretion rate of $4.0 \times 10^{-6} M_{\odot} \text{ yr}^{-1}$ and a $2.0 M_{\odot}$ central object, Hanami's model predicts the energy from a single outburst is of order 10^{47} ergs. The combined kinetic energy of the clumps observed in the outflow is $\sim 2.0 \times 10^{44}$ ergs, suggesting that such an outburst may be capable of producing them.

More sensitive, higher resolution observations of these clumps would be very useful to further constrain acceleration and expansion models and the nature of the blobs themselves.

V. SUMMARY

The region surrounding IRAS 1629A was mapped in the $^{12}\text{CO } J = 2 \rightarrow 1$ transition. A single $^{13}\text{CO } J = 2 \rightarrow 1$ spectra was also taken toward the IR source. The principal results are the following.

1. The $^{12}\text{CO } J = 2 \rightarrow 1$ observations in the vicinity of IRAS 1629A made with $27''$ resolution indicate the presence of four emission lobes.

2. The morphology and velocity structure of the lobes suggests that there are two separate outflow systems, although, other interpretations are possible. In the two outflow model, the outflow axes have position angles of $\sim 51^\circ$ and 95° . The more confined of the two outflows is roughly aligned with the position angle of the local magnetic field.

3. The mass and mechanical luminosity of the redshifted material in the outflow were calculated. The outflow system was found to have a low mass ($M < 1 M_{\odot}$) and luminosity ($L \sim 2 L_{\odot}$).

4. There is evidence in three of the four lobes that the highest velocity emission comes from clumps of gas that are either being continuously accelerated from low to high velocities along the length of the outflow or are undergoing a free-flow expansion as the result of an explosive event in the outflow's past. The clumps range in mass from $\sim 10^{-2}$ to $10^{-3} M_{\odot}$. For the acceleration to occur the clumps must be moving through a low-density (less than 10^3 cm^{-3}) or an evacuated cavity. The acceleration could be produced by a stellar wind driven by a mass-loss rate greater than $10^{-6} M_{\odot} \text{ yr}^{-1}$. The free-flow expansion of clumps could be explained by variations in the accretion rate which has resulted in a FU Orionis type of outburst.

We wish to thank the NRAO staff for their help during the observational and data reduction phases of this project. We also thank R. Levreault for his helpful comments and suggestions.

This work was supported in part by the IRAS Data Analysis program under JPL contract 957396.

REFERENCES

- Bally, J., and Lada, C. J. 1983, *Ap. J.*, **265**, 824.
 Cabrit, S., and Bertout, C. 1986, *Ap. J.*, **307**, 313.
 Dickman, R. L. 1978, *Ap. J. Suppl.*, **37**, 407.
 Fridlund, C. V. M., Sandqvist, A., Nordh, H. L., and Olofsson, G. 1984, *Astr. Ap.*, **137**, L17.
 Fukui, Y., Sugitani, K., Takaba, H., Iwata, T., Mizuno, T., Ogawa, H., and Kawabata, K. 1986, *Ap. J. (Letters)*, **311**, L85.
 Goldsmith, P. F., Snell, R. L., Hemeon-Hager, M., and Langer, W. D. 1984, *Ap. J.*, **286**, 599.
 Hanami, H. 1987, preprint.
 Hartmann, L., and Keyon, S. J. 1985, *Ap. J.*, **289**, 331.
 Hayashi, S. S., Hayashi, M., Uchida, Y., Kaifu, N., Hasegawa, T., and Shibata, K. 1987, in *IAU Symposium 115 Star Forming Regions* ed M. Peimbert and J. Jugaku (Dordrecht: Reidel) p. 348.
 Herbig, G. H. 1977, *Ap. J.*, **217**, 693.
 Kutner, M. L., and Ulich, B. L. 1981, *Ap. J.*, **250**, 341.
 Lada, C. J. 1985, *Ann. Rev. Astr. Ap.*, **23**, 267.
 Lada, C. J., and Harvey, P. M. 1981, *Ap. J.*, **254**, 58.
 Levreault, R. M. 1983, *Ap. J.*, **265**, 855.
 Margulis, M., and Lada, C. J. 1985, *Ap. J.*, **299**, 925.
 Menten, K. M., Serabyn, E., Gusten, R., and Wilson, T. L. 1987, preprint.
 Moriarty-Schieven, G. H., Snell, R. L., Strom, S. E., Schloerb, F. P., Strom, K. M., and Grasdalen, G. L. 1987, *Ap. J.*, **319**, 742.
 Mundy, L. G., Wilking, B. A., and Myers, S. 1986, *Ap. J. (Letters)*, **311**, L75.
 Pudritz, R. E., and Norman, C. A. 1983, *Ap. J.*, **274**, 677.
 Snell, R. L., Loren, R. B., and Plambeck, R. L. 1980, *Ap. J. (Letters)*, **239**, L17.
 Snell, R. L., Scoville, N. Z., Sanders, D. B., and Erickson, N. R. 1984, *Ap. J.*, **284**, 176.
 Uchida, Y., and Shibata, K. 1985, *Pub. Astr. Soc. Japan*, **37**, 515.
 Ulich, B. L., and Haas, R. W. 1976, *Ap. J. Suppl.*, **30**, 247.
 Vrba, F. J., Strom, S. E., and Strom, K. M. 1976, *A.J.*, **81**, 958.
 Walker, C. K., Lada, C. J., Young, E. T., and Maloney, P. R. 1988, preprint.
 Walker, C. K., Lada, C. J., Young, E. T., Margulis, M., and Wilking, B. A. 1985, *Bull. AAS*, **17**, 835.
 Walker, C. K., Lada, C. J., Young, E. T., Maloney, P. R., and Wilking, B. A. 1986, *Ap. J. (Letters)*, **309**, L47.
 Wootten, A., and Loren, R. B. 1987, *Ap. J.*, **317**, 220.

CHARLES J. LADA, CHRISTOPHER K. WALKER, and ERICK T. YOUNG: Steward Observatory, University of Arizona, Tucson, AZ 85721

MICHAEL MARGULIS: FCRAO, University of Massachusetts, Graduate Research Center, Tower B, Amherst, MA 01003